CALPHAD: Computer Coupling of Phase Diagrams and Thermochemistry 35 (2011) 455–462

Contents lists available at SciVerse ScienceDirect

CALPHAD: Computer Coupling of Phase Diagrams and Thermochemistry

journal homepage: www.elsevier.com/locate/calphad

Effect of inclusions on the solidification structures of ferritic stainless steel: Computational and experimental study of inclusion evolution

Joo Hyun Park*

School of Materials Science and Engineering, University of Ulsan, Ulsan 680-749, Republic of Korea

ARTICLE INFO

Article history:
Received 29 April 2011
Received in revised form
29 July 2011
Accepted 7 August 2011
Available online 2 September 2011

Keywords:
Equiaxed solidification structure
Ferritic stainless steel
Disregistry
Thermochemical computation
Bimodal distribution
Inoculant

ABSTRACT

The effect of oxide and nitride inclusions in a steel melt on the formation of the equiaxed grain structure during solidification of ferritic stainless steel has been investigated. The solidified grain size decreased with an increasing content of titanium. In steel samples with large solidified grains, the inclusions were generally a two-phase system in which the titanium oxide was precipitated in the liquid TiO_x–Cr_2O_3–SiO_2 matrix during cooling. Alternatively, in steel samples with fine equiaxed grains, single TiN and $MgAl_2O_4$–TiN complex particles were observed. MgO–Al_2O_3–TiO_x ternary compounds formed in molten steel, and the spinel crystals grew at the expense of the liquid phase as the temperature decreased. Concurrently, the TiN nucleated on the surface of the $MgAl_2O_4$ particles because the lattice disregistry between $MgAl_2O_4$ and TiN was low. The formation behaviors of non-metallic compounds were successively predicted via thermochemical computation. Single mode log-normal distributions with mode particle diameters (d_{mode}) were observed in many samples, whereas a bimodal distribution was obtained in solidified samples with a fine-grained equiaxed structure. The grain sizes of the solidified samples decreased when the mean diameter of the inclusions increased. Consequently, the solidification structure can be interpreted based on the effectiveness of TiN and $MgAl_2O_4$–TiN complex inclusions as inoculants for the nucleation of δ-Fe.

1. Introduction

Ferritic stainless steel (FSS) sheets develop an undesirable surface corrugation known as ridging when pulled or deeply drawn [1–11]. The resulting FSS exhibits undulation, with peaks on one side of the sheet coinciding with valleys on the other side, without a change in the thickness. The ridges have a depth of 20–50 μm and the undesirable surface defect adds manufacturing costs through the need for polishing. Therefore, many scientists have investigated the causes and countermeasures using the finite element method [4,5], electron back scatter diffraction analysis [7,9,10], recrystallization technology [8], and intermediate annealing technology [12]. However, because the solidified structure is one of the most critical factors affecting the texture and thus the ridging phenomenon of FSS sheets [6], the columnar-to-equiaxed transition (CET) during the solidification process has been investigated in order to obtain an equiaxed grain structure of FSS [13–15]. There have been several trials to apply the electromagnetic stirring technology, to control the superheating or undercooling, and to control the casting speed [14–18]. However, these parameters are generally controlled within a very narrow operational window during the continuous casting process with regard to the stability and production rate of a daily operation.

Alternatively, the grain refinement of the solidification structure of steel welds has been investigated for mechanical properties, such as strength and toughness [19–21]. There are several reports elucidating the effect of titanium on the refinement of the solidified grain of the weld pool of FSS. The addition of titanium resulted in the formation of titanium-rich oxide and nitride in the liquid phase. These particles could become heterogeneous nucleation sites of delta-ferrite during solidification. Villafuerte et al. [22] found that the fraction of the equiaxed grain increased with increasing titanium content above 0.18 mass% and increased by increasing the content of aluminum at a given level of titanium in gas-tungsten-arc (GTA) welds in FSS containing 11–32 mass% Cr. The positive effect of Al_2O_3 on the grain refinement of steel welds was also reported by Kluken et al. [23]. Titanium–rich cuboidal (oxide) inclusions were also found to contain Al–Ca–Mg-rich oxide phases at their centers. Villafuerte et al. [24] performed more systematically designed experiments to examine the mechanisms for providing nuclei to equiaxed grains in GTA welds in FSS (11–17 mass% Cr) and found that TiN particles acted as heterogeneous nucleation sites that were originally documented by Bramfitt [25]. However, no evidence for equiaxed grain formation by dendrite fragmentation was observed, despite the fact that Ti addition did produce a more highly branched dendritic structure. However, recently, the Monte

* Tel.: +82 52 259 2227; fax: +82 52 259 1688.
E-mail address: basicity@mail.ulsan.ac.kr.

0364-5916/$ – see front matter © 2011 Elsevier Ltd. All rights reserved.
doi:10.1016/j.calphad.2011.08.004

Table 1
Compositions of steel samples in the present study (mass%).

Sample no.	Composition of steel samples in the present study (mass%)								Grain size (mm)	d_v (um)
	Cr	Si	Mn	O	N	Ti	Al	Mg		
0	11.1	0.47	0.29	0.0023	0.013	0.036	0.0035	0.0007	1.73	3.60
1	11.2	0.46	0.28	0.0029	0.008	0.023	0.0035	0.0004	2.14	3.50
2	11.1	0.44	0.29	0.0018	0.010	0.035	0.0045	0.0004	2.25	3.20
3	11.1	0.49	0.29	0.0023	0.010	0.020	0.0020	0.0003	3.46	2.50
4	11.1	0.49	0.28	0.0024	0.012	0.013	0.0020	0.0004	2.50	2.81
5	11.1	0.51	0.29	0.0024	0.013	0.015	0.0021	0.0004	3.21	2.70
6	11.0	0.46	0.28	0.0030	0.015	0.010	0.0020	0.0004	3.46	2.80
7	11.0	0.59	0.28	0.0032	0.016	0.071	0.0074	0.0003	1.88	3.89
8	11.0	0.59	0.29	0.0023	0.021	0.100	0.0113	0.0003	1.05	4.16
9	11.0	0.60	0.29	0.0024	0.013	0.029	0.0045	0.0003	2.65	3.00
10	11.0	0.62	0.28	0.0025	0.015	0.024	0.0043	0.0003	2.81	3.20
5-1	11.1	0.40	0.28	0.0034	0.016	0.005	0.0017	0.0004	4.50	2.54

Carlo method illustrated that the melt undercooling increased with the addition of soluble titanium during weld solidification in FSS (17–19 mass% Cr) [26]. Hence, the equiaxed grain formation was promoted not only by a nucleating agent, TiN, but by melt undercooling, and both were requisite for CET.

Even though there was no objection to the role of TiN during crystallization of primary delta-ferrite, the effect of aluminum and its oxide on grain refinement has not been clarified. Fujimura et al. [27] found that when the Mg/Al mass ratio of oxides covered by TiN ranged from 0.3 to 0.5, an equiaxed fine-grain structure was produced in 16 mass% Cr FSS. Therefore, in the present study, we investigated the effects of MgO–Al_2O_3 oxide and TiN inclusion particles, formed in-situ by addition of Al and Ti, in a steel melt on the formation of equiaxed grains during solidification of FSS. Further, the evolution and the phase equilibria of oxide and nitride inclusions have been predicted using a thermochemical computing program.

2. Experimental procedure

Pure Fe, Cr, Si, and Mn (>99.99 mass% reagent grade) were premelted in a vacuum induction furnace to produce a nominal composition of Fe-11 mass% Cr-0.5 mass% Si-0.3 mass% Mn FSS. Alloys of approximately 730 g and premelted CaO–SiO_2–MgO–Al_2O_3–4 mass% CaF_2 ((mass% CaO + mass% MgO)/(mass% SiO_2 + mass% Al_2O_3) = 0.9–1.7) fluxes of approximately 30 g were equilibrated in pure MgO (>99.9 mass%, MgO–S(3N), TEP Corp., Tokyo, Japan) crucibles (ID; 45 mm, OD; 53 mm, HT; 130 mm) at 1873 K. The initial contents of dissolved aluminum and titanium in the premelted alloy were less than 25 mass ppm.

The quartz reaction chamber was initially evacuated using a mechanical rotary pump and was then filled with an Ar-3 vol% H_2 gas mixture and induction heated. The temperature was set to 1873 K using an *R*-type (Pt-13 mass% Rh/Pt) thermocouple and a proportional integral differential controller. Any possible interference of high frequency on the temperature detection was reduced by grounding the circuit of the thermocouple. Preliminary trials confirmed that the radio frequency interference was not significant in the present experimental setup, and the temperature fluctuation of steel melts was controlled to ±3 K during the experiments. Even though 99.999% purity Ar gas was used, the oxygen in the Ar gas was removed by passing the gas through magnesium turnings heated to 773 K. After the steel samples were melted at 1873 K, the premelted fluxes were added, followed by the addition of less than 200 mass ppm Al. After 3 min, a fixed amount of Ti equivalent to 0.3 mass% was added. All of the additives, including fluxes and metals, were dropped through the quartz tube under an Ar-3 vol% H_2 atmosphere. The system was then equilibrated for 60 min, after which the furnace was turned off, and the resulting cooling rate was 65 K/min until the temperature reached 1673 K. A schematic diagram of the experimental apparatus is shown in Fig. 1.

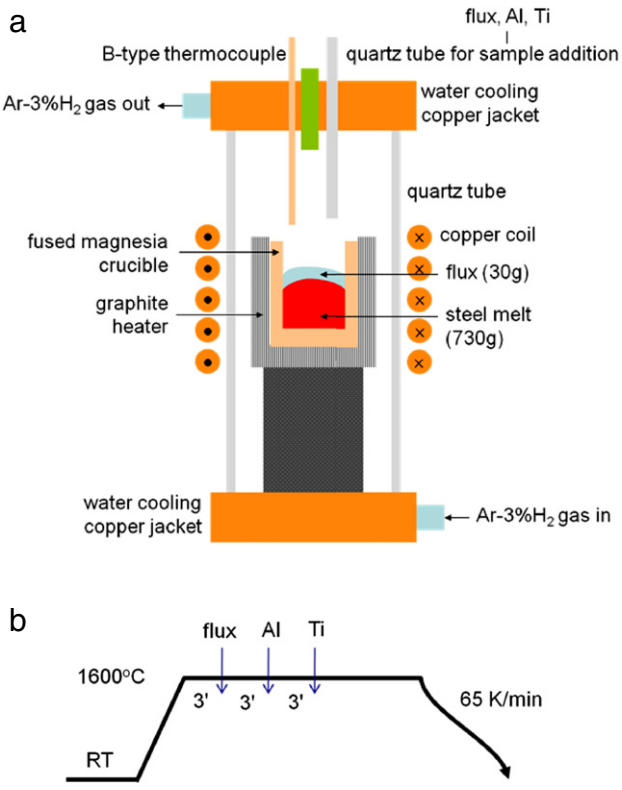

Fig. 1. Schematics of the experimental apparatus (a) and the experimental methods including flux/alloy addition, sampling and cooling of steel samples (b).

The metal samples were prepared for chemical analysis. The major components such as Cr, Si, and Mn were analyzed using optical emission spectrometry, and the contents of Al, Ti, and Mg were determined via inductively-coupled plasma spectroscopy (ICP-AES, IRIS Advantage (REG), Thermo Electron, Waltham, MA). The contents of oxygen and nitrogen were analyzed via fusion and the infrared absorption method after very careful preparation through ultrasonic cleaning. The final FSS compositions are listed in Table 1.

The macroscopic scale grain sizes of the solidified alloys were measured using an optical microscope. The size distributions, morphologies, and compositions of the inclusion particles were measured using a scanning electron microscope equipped with an energy dispersive spectroscope (SEM-EDS, JSM-840A, JEOL) with a link detector and an automatic image analysis system.